International Journal of Nanoscience

NEAR-FIELD RAMAN SPECTROSCOPY OF INDIVIDUAL SINGLE-WALLED CARBON NANOTUBES

Achim Hartschuh

Physical and Theoretical Chemistry, Universität Siegen
Siegen, 57068,Germany

Neil Anderson

Lukas Novotny

The Institute of Optics, University of Rochester
Rochester, NY 14627, USA

Received (Day Month Year)
Revised (Day Month Year)

Near-field Raman spectroscopy with high spatial resolution is used to study single-walled carbon nanotubes (SWNT) within dense samples. A sharp, laser irradiated metal tip acts as a near-field excitation source causing an enhanced Raman signal within close proximity of the tip. We present optical images of different Raman modes with a spatial resolution better than 15 nm. Local spectroscopy allows us to identify and distinguish tubes with different structures on the nanometer-scale and to observe variations within the spectrum of individual tubes.

Keywords: Near-field Raman spectroscopy; Single-walled Carbon Nanotubes; Nanooptics.

1. Introduction

The prospects of carbon nanotubes as building blocks for future carbon nanotube based devices depend crucially on the development of new strategies for their structural-selective growth, separation, manipulation and structural analysis. While significant progress has been made regarding tube production and separation (see e.g. [1,2], no method resulting in particular tube structures on demand has been realized so far. Furthermore, many applications, such as field-effect transistors (FET) or non-volatile memory devices, demand high density assemblies of tubes requiring new techniques for nanoscale analysis with single tube sensitivity.

Raman spectroscopy has been demonstrated to provide both chemical specificity and sensitity. By probing the radial breathing mode (RBM) frequency and making use of resonance Raman enhancement the identification of the structural parameters (n,m) of a SWNT can be achieved e. g. [3,4,5,6,7,8].

All of this work has been done using standard confocal microscopy where the diffraction barrier limits the achievable resolution to about $\lambda/2$. In order to study

individual tubes, the sample coverage had to be fairly low, smaller than 1 tube per μm^2. Recently, we demonstrated near-field Raman imaging of individual SWNT with sub 30 nm spatial resolution [9,10,11]. Tip-enhanced Raman spectroscopy has been proposed already in [12] and has been demonstrated experimentally by different groups (see e. g. [13,14,15,16]).

In this paper, we apply this technique to perform local spectroscopy of different Raman modes including the RBM and investigate nano-scale features of SWNT. Furthermore, the field enhancement achieved at the end of the tip is shown to provide an enormous amplification of the Raman signal.

2. Experimental

Our experimental setup is shown schematically in fig. 1. It is based on a confocal microscope in combination with a probe head for shear-force detection.

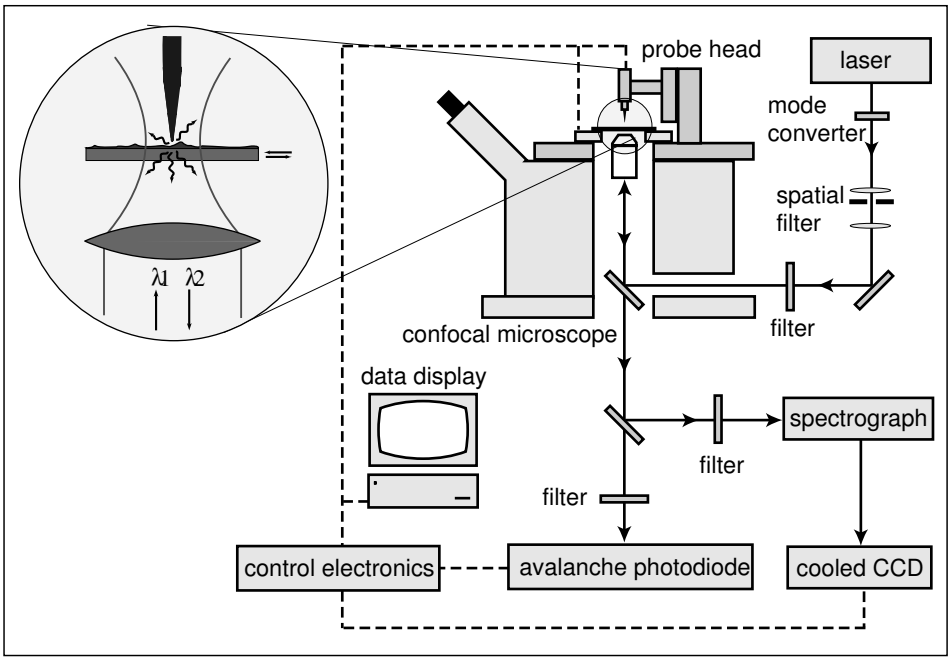

Fig. 1. Schematic of the experimental setup. A sharp metal tip is positioned above a carbon nanotube sample and centered into a tightly focused radially polarized laser beam. An optical scan image is obtained by laterally scanning the sample using a (x,y)-scan stage. The optical signal is detected either after spectral filtering by an avalanche photodiode (APD) or by a combination of a spectrograph and a CCD.

The laser excitation is provided by a HeNe laser operating at 632.8 nm (P = 15 mW, TEM_{00}). The laser output is expanded and converted into a radially polarized beam by passing through a mode converter followed by spatial filtering.

The mode-converter used consists of four pieces of a $\lambda/2$-plate for 632.8 nm, cut and recombined appropriately as described in [17]. The beam is attenuated to 30 - 100μW and sent into the microscope after passing a laser line filter. The beam is reflected by a dichroic beam splitter and focused by a high numerical aperture objective (1.4 NA) on the sample surface. The tip is positioned above the nanotube sample and centered into the laser focus where the longitudinal field induces the local field enhancement effect [18]. The Raman scattered light is collected with the same objective, transmitted by the beam splitter and filtered by a long pass filter. The signal is detected either by a combination of a spectrograph and a charge coupled device (CCD) or by a photon-counting avalanche photodiode after spectral filtering using a narrow band pass filter (FWHM = 10 nm) centered at 760 nm or 700 nm, respectively.

The metal tip is held within 2 nm above the sample surface by using a tuning-fork feedback mechanism [19]. Typical interaction forces between tip and sample are in the range of 10- 50 pN, small enough to not affect the tip shape. This soft interaction is achieved by using a tuning fork with high quality factor for oscillation and by keeping the frequency detuning constant with a digital phase-locked loop. Sharp gold tips with a radius of curvature around 15 nm are produced by electrochemical etching in hydrochloric acid .

Purified single-walled carbon nanotubes produced by arc-discharge using nickel/yttrium catalyst particles, were used as purchased from BuckyUSA. The material was dispersed in dichlorethane, sonicated for 1h and spin-cast on a microscope cover glass. The sample was mounted on a 40 x 40 μm closed-loop scan bed.

3. High-resolution imaging of SWNT

Figure 2(a) shows the near-field Raman image of SWNTs on glass in a 2 x 2 μm^2 scan area established by detecting the intensity of the G band upon laser excitation at 632.8 nm. In fig. 2(b), the simultaneously acquired topography image of the sample is presented. Cross sections taken along the dashed lines in fig. 2(a) and (b) are shown in (c) and (d) for the optical and the topographic images, respectively. The minimal width of the observed optical features is about 20 nm, far below the diffraction limit of light at this wavelength.

The optical and topographic images are closely correlated and the SWNTs can be easily identified. In some cases, however, tubes that are observed topographically do not exhibit a detectable Raman signal. The Raman scattering strength of tubes is known to be strongly dependent on the energy difference between photon energies and the electronic energies of the tube. This *resonance Raman* effect enhances the signal essentially and is the reason why even single tubes can be observed [4]. Non-resonant tubes at 632.8 nm are Raman-inactive and do not appear in the optical image in fig. 2(a) [20].

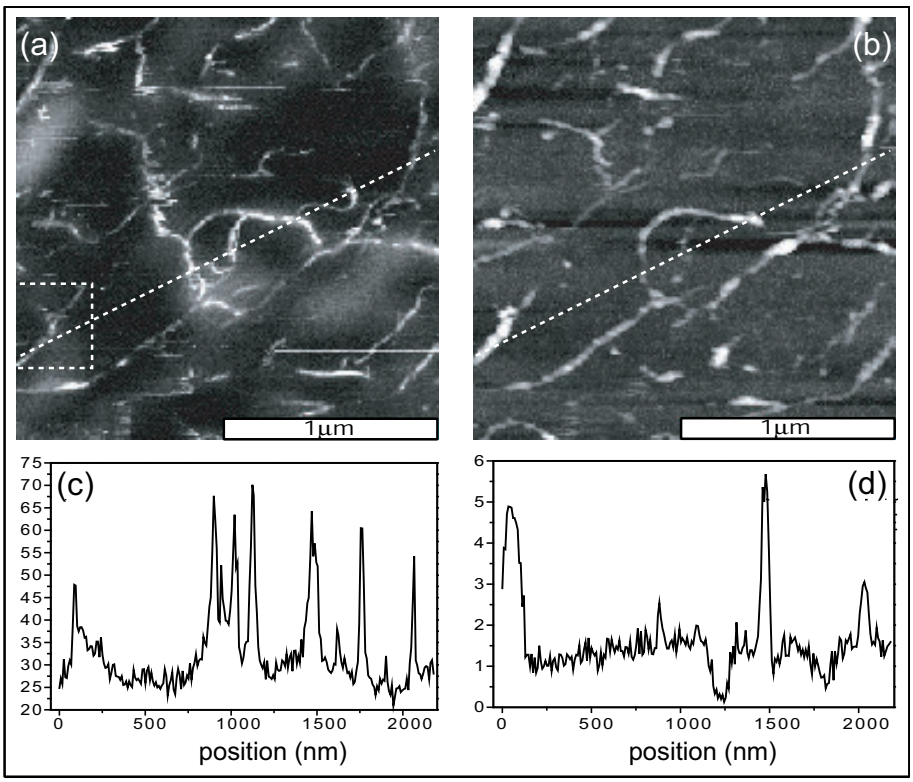

Fig. 2. Simultaneous near-field Raman image (a) and topographic image (b) of SWNTs on glass. Scan area 2 x 2 μm^2. The Raman image is acquired by detecting the intensity of the G band upon laser excitation at 632.8 nm. (c) Cross section taken along the indicated dashed line in the Raman image. (d) Cross section taken along the indicated dashed line in the topographic image. Vertical units are 1000 photon counts per second for (c) and nanometer for (d).

4. Nanoscale Spectroscopy of SWNT

The near-field Raman image presented in fig. 2(a) reveals an inhomogeneous sample coverage with a series of bright features. The high spatial resolution of $\approx$ 20 nm achieved by the tip-enhanced technique implies that the detected Raman signal originates from a sample area of about 20 nm in diameter. Besides providing images with unprecedented spatial resolution, this technique opens up the possibility to perform local spectroscopy of SWNTs on the nanoscale.

A more detailed analysis of the SWNT material is demonstrated as an example for the sample area marked by a white square in fig. 2(a). First, it was studied using a smaller scan range of 400 nm x 400 nm. The measured image, presented in figure 3(b), exhibits a very bright feature with a size of approx. 40 nm x 20 nm. To explore the origin of this feature, a near-field Raman spectrum using the sharp metal tip was measured shown in fig. 3(a) (black curve). Besides the characteristic

and sharp G band at 1592 cm^{-1}, a broader band with maximum at 1550 cm^{-1} is observed that is commonly attributed to arise from a Breit-Wigner-Fano (BWF) resonance in metallic SWNT [21]. In the farfield spectrum without tip (grey curve in fig. 3)(a) the observed signal is much weaker and the BWF contribution is nearly absent. This difference can be understood by considering the different areas probed in near-field and farfield. The near-field signal originates from a circular sample area of about 20 nm shown schematically in fig. 3(b) as a small white circle, whereas the farfield signal is produced within a diffraction limited spot of about 300 nm (large, dotted white circle in fig. 3(b)). The farfield spot gives rise to an observed spectrum that represents an average over all the SWNTs within the spot area. Since the farfield spectrum does not exhibit a BWF-band, we conclude that most of the tubes within the farfield area are semiconducting. The BWF-band is transmitted by the bandpass filter used to acquire the image shown in fig. 3(b). We thus attribute the origin of the bright feature to a short (40 nm) metallic nanotube.

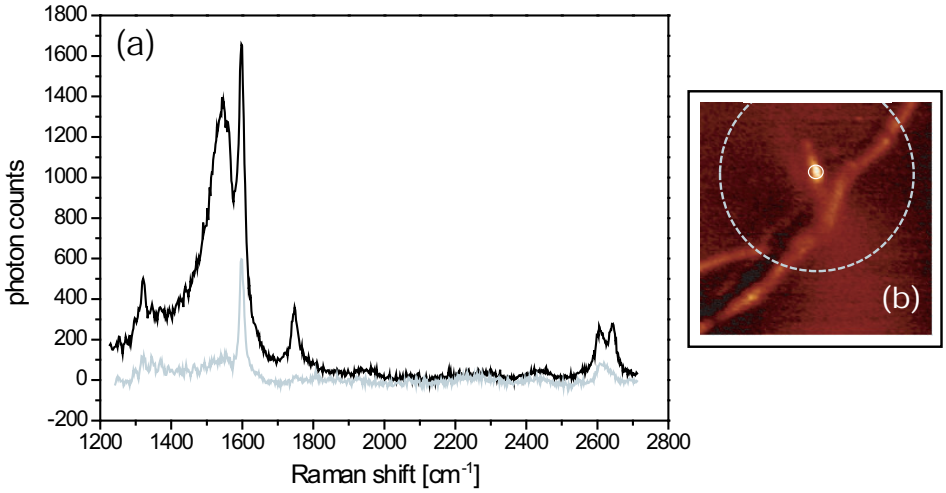

Fig. 3. (a) Raman spectra detected on top of the bright feature marked in (b): With metal tip (black curve) and without tip (grey curve). (b) Near-field Raman image showing the intensity of the G band. Scan area 400 nm x 400 nm. The white circles indicate the areas probed in the near-field (solid line) and farfield (dashed line).

5. Structural identification of SWNT on the nanoscale

The structural identification of SWNTs using Raman scattering has been discussed by various groups. It relies in general on the observation of the diameter dependent radial breathing mode (RBM) frequency ν_{RBM} The energy of the RBM is taken to be inversely proportional to the diameter $\nu_{RBM} = \alpha d^{-1} + \beta$ [22]. The exact value of α and β varies slightly between different theoretical models and experiments.

The high resolution near-field technique presented can be used for local measurements of the RBM frequencies and thus for the identification of the tube structure

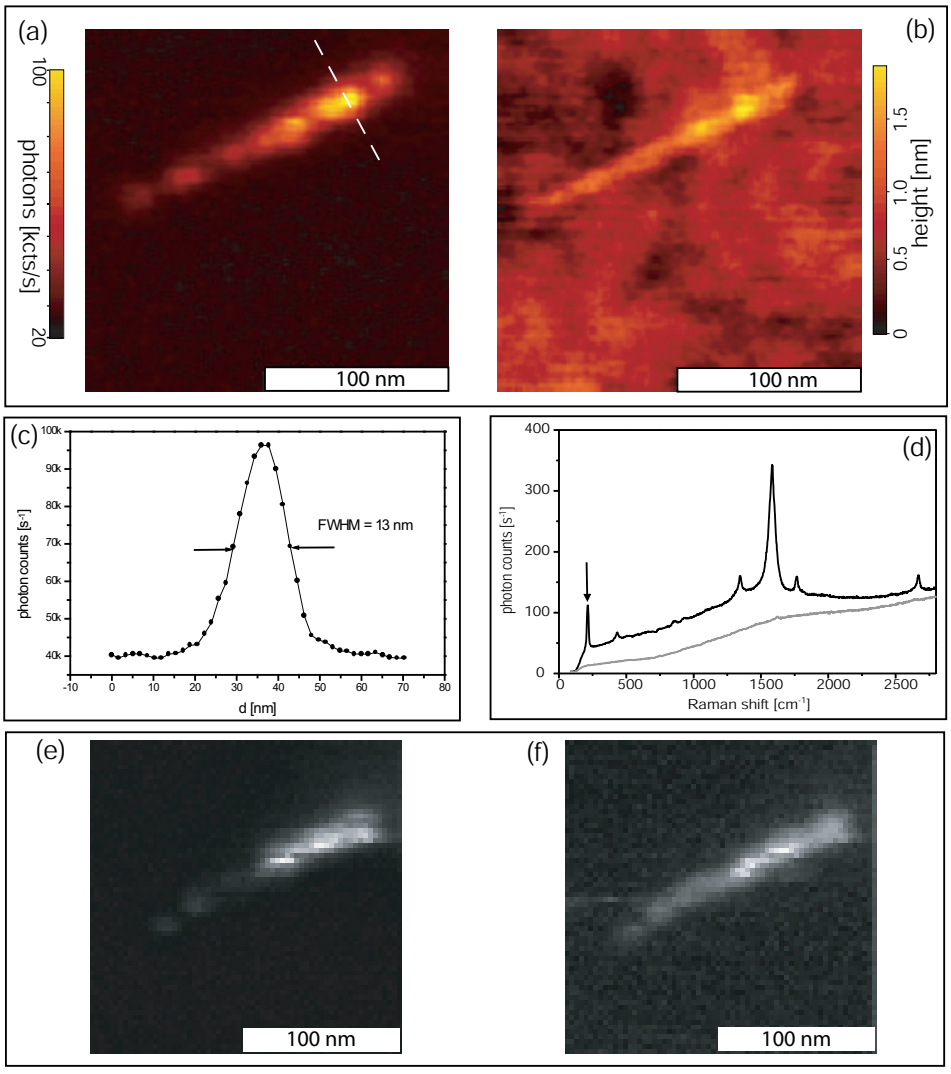

Fig. 4. Structural identification of a SWNT with ultrahigh spatial resolution. (a) and (b) Simultaneous Raman and topographic images (the darker areas in the topography image reflect terraces of different hight within the glass substrate). (c) Cross-section through the optical image along the dashed line in (a) showing a width of 13 nm. (d) Near-field Raman spectrum detected on top of the SWNT at the position marked in (b). The arrow markes the position of the radial breathing mode signal at 199 cm^{-1} indicating a tube diameter of 1.2 nm. The structure (n, m) of the SWNT is presumably (14,2) (see text). (e) and (d) Near-field Raman images established by detecting selectively the spectral range of the RBM band (190 - 209 cm^{-1}) and the D band (1255 - 1370 cm^{-1}) respectively.

with nanoscale accuracy. The RBM frequencies have been selectively measured for certain positions along the SWNTs shown in Fig. 4. The figure shows a topographic image and a simultaneously acquired near-field Raman image using the intensity of the G-band. The intensity of the G-band is inhomogeneous along the tube and the signal becomes clearly weaker in the lower part of the image.

The optical cross section, shown in fig. 4(c), exhibits a feature with a width of only 13 nm (FWHM). The observed tube height in fig. 4(b) of about 1.2 nm corresponds presumably to the diameter of the tube. Since the width of the optical signal is larger than the width of its source, 13 nm vs. 1.2 nm, it represents the optical resolution of our setup. As in atomic force microscopy (AFM), the spatial resolution of our technique is directly determined by the diameter of the tip apex. With decreasing tip radius, the lateral confinement of the enhanced field becomes stronger [18,12] and the optical resolution is improved. By optimizing the etching procedure, sharpers tips could be fabricated and optical resolutions down to 1 nm could become feasible.

Fig. 4(d) shows the tip-enhanced Raman spectrum detected on top of the tube (black curve) and the spectrum without tip (grey curve) both acquired using an integration time of 10 s. While the tip-enhanced spectrum exhibits clear Raman peaks with excellent signal to noise ratio, the Raman signal is hardly observed in the non-enhanced spectrum. By comparing the intensities of the G-band for both spectra, a lower limit for the signal enhancement of about 2500 is found.

In the tip-enhanced spectrum, a clear RBM peak is observed at 199 cm^{-1}. Using the relationship $\nu_{RBM}(cm^{-1}) = 223.5d^{-1}(nm) + 12.5$ a diameter of 1.2 nm is determined that corresponds to the resonant tube structure (n,m)= (14,2) [7]. To obtain a RBM-image of the tube-sample the intensity of the Raman scattering spectrum has been integrated over the range $\nu = [190\,..\,205]$ cm^{-1} (fig. 4(e)). We observe that the position of the RBM is constant along the tubes indicating a uniform tube diameter. While both, RBM and G band show weaker contributions within the lower half of the tube, the D band intensity appears to be more uniform with a peak in the middle of the tube. Although we can clearly image and analyze the relevant Raman signals including RBM, D-, G' and G-band, a further discussion of the near-field image contrast is not possible because of the non-uniform sample topography (fig. 4(b)).

6. Summary

In this contribution, we demonstrated tip-enhanced Raman imaging and spectroscopy of SWNT on glass with an unprecedented optical resolution of sub 15 nm. Besides the increased optical contrast, the Raman signal is enhanced by a factor of about 2500 providing an enormously increased detection sensitivity. Combining the high spatial resolution with the chemically specificity of Raman spectroscopy, the structural analysis of high density SWNT coverage is made possible.

Acknowledgments

The authors wish to thank M. Beversluis and A. Bouhelier for stimulating discussions and experimental support. This work was supported by AFOSR through grant F-49620-03-1-0379

References

References

1. Krupke, R., Hennrich, F., Löhneysen, H. v., and Kappes, M. M., *Science*, **301**, 344 (2003).
2. Zheng, M., Jagota, A., Strano, M. S., Santos, A. P., Barone, P., Chou, S. G., Dinder, B. A., Dresselhaus, M. S., Mclean, R. S., Onoa, G. B., Samsonidze, G. G., Semke, E. D., Usrey, M., and Walls, D. J., *Science*, **302**, 1545 (2003).
3. Rao, A. M., Richter, E., Bandow, S., Chase, B., Eklund, P. C., Williams, K. A., Fang, S., Subbaswamy, K. R., Menon, M., Thess, A., Smalley, R. E., Dresselhaus, G., and Dresselhaus, M., *Science*, **275**, 187 (1997).
4. Jorio, A., Saito, R., Hafner, J. H., Lieber, C. M., Hunter, M., McClure, T., Dresselhaus, G., and Dresselhaus, M., *Phys. Rev. Lett.*, **86**, 1118 (2001).
5. Kuzmany, H., Plank, W., Hulman, M., Kramberger, C., Grüneis, A., Pichler, T., Peterlik, H., Kataura, H., and Achiba, Y., *Eur. Phys. J. B*, **22**, 307 (2001).
6. Reich, S., Thomsen, C., and Maultzsch, J., *Carbon nanotubes*, Wiley-VCH, Weinheim, 2004.
7. Bachilo, S. M., Strano, M. S., Kittrell, C., Hauge, R. H., Smalley, R., and Weisman, R. B., *Science*, **298**, 2361 (2002).
8. Hartschuh, A., Pedrosa, H. N., Novotny, L., and Krauss, T. D., *Science*, **301**, 1354 (2003).
9. Hartschuh, A., Sánchez, E. J., Sunney, X. S., and Novotny, L., *Phys. Rev. Lett.*, **90**, 095503 (2003).
10. Hartschuh, A., Beversluis, M. R., Bouhelier, A., and Novotny, L., *Philosophical Transactions: Mathematical, physical and engineering science*, pp. 807–819 (2004).
11. Hartschuh, A., Anderson, N., and Novotny, L., *J. Microscopy.*, **210**, 234 (2003).
12. Wessel, J., *J. Opt. Soc. Am. B*, **2**, 1538 (1985).
13. Stöckle, S. M., Suh, Y. D., Deckert, V., and Zenobi, R., *Chem. Phys. Lett.*, **318**, 131 (2000).
14. Hayazawa, N., Inouye, Y., Sekkat, Z., and Kawata, S., *Chem. Phys. Lett.*, **335**, 369 (2001).
15. Nieman, L. T., Krampert, G. M., and Martinez, R. E., *Rev. Sci. Instrum.*, **72**, 1691 (2001).
16. Pettinger, B., Ren, B., Picardi, G., Schuster, R., and Ertl, G., *Phys. Rev. Lett.*, **92**, 096101 (2004).
17. Quabis, S., Dorn, R., Glöckl, O., Eberler, M., and Leuchs, G., *Opt. Comm.*, **179**, 1 (2000).
18. Novotny, L., Sánchez, E. J., and Xie, X. S., *Ultramicroscopy*, **71**, 21 (1998).
19. Karrai, K., and Grober, R. D., *Appl. Phys. Lett.*, **66**, 1842 (1995).
20. Jiang, C., Zhao, J., Therese, H. A., Friedrich, M., and Mews, A., *J. Phys. Chem. B*, **107**, 8742 (2003).
21. Pimenta, M. P., Marucci, A., Empedocles, S. A., Bawendi, M. G., and Hanlon, E. B., *Phys. Rev. B*, **58**, R16016–R16019 (1998).

22. Jishi, R. A., Venkataraman, L., Dresselhaus, M. S., and Dresselhaus, D., *Chem. Phys. Lett.*, **209**, 77–82 (1993).